Electronic Supplementary Material (ESI) for Environmental Science: Water Research & Technology.

SUPPORTING INFROMATION

for

Comparing Energy Demands and Longevities of Membrane-based Capacitive Deionization Architectures

Vineeth Pothanamkandathil and Christopher A. Gorski*

Department of Civil and Environmental Engineering, The Pennsylvania State University,
University Park, PA 16802, USA

*Corresponding author: Email: gorski@psu.edu; Tel: +1 814-865-5673

The supporting information contains 11 pages, 5 sections, 7 figures, and 1 table.

Section S1. Procedure for flow-cell assembly, deionization experiments, longevity tests, and electrochemical impedance spectroscopy tests.

Deionization Experiments:

MCDI architecture: The flow-cell was assembled by placing the electrode-current collector assemblies atop the endplates. A thin silicone gasket (200 μm) was placed over the endplate and electrode to secure the electrode in place. An anion exchange membrane (70 ± 5 μm, Fumasep FAS-PET-75, FuMA-Tech, Germany) was placed over one electrode, and a cation exchange membrane (75 ± 5 μm, Fumasep FKD-PK-75, FuMA-Tech, Germany) was placed over the other. A 150 μm polycarbonate gasket and PTFE spacer were sandwiched between the two endplate assemblies to form the flow channel for the desalinating stream. A sectional view of the MCDI setup is provided in **Figure S1**. A flow-through conductivity electrode (ET908 Flow-Thru Conductivity Electrode, eDAQ, Australia) were placed at the outlet to measure the conductivity of the deionized effluent.

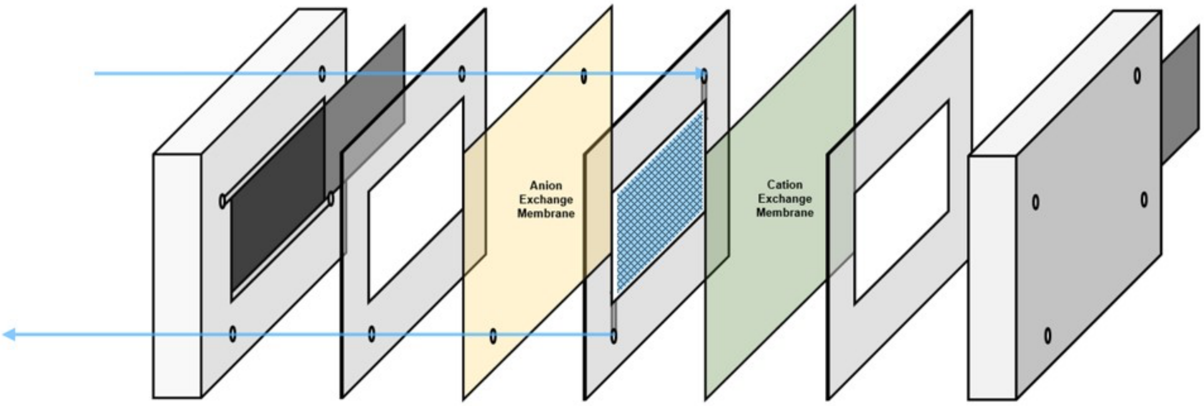

Figure S1. Sectional view of flow-cell setup for the membrane capacitive deionization (MCDI) experiments. The blue arrows represent the flow path for the desalinating stream.

For the deionization experiments, 20 mM NaCl solution was flowed through the desalinating stream (the blue arrows represent the flow path of the desalinating stream, **Figure S1**). As the 20 mM NaCl solution flowed through the desalinating stream, a constant current was applied using a potentiostat (BioLogic MG 2.5, France, respectively) to the flow-cell until a predetermined cut-off voltage was achieved. After reaching the cut-off voltage the direction of the applied current was switched.

MC-MCDI architecture: The endplate assemblies were similar to that of the MCDI setup, with the only difference being that a thicker silicone gasket (1.5 mm) was used to secure the electrode and a PTFE spacer was placed atop the electrode before placing the ion-exchange membranes to form the outer channels. The deionization stream was formed by sandwiching a polycarbonate gasket (150 μm) and a spacer between the endplate assemblies as shown in **Figure S2**. The flow-through conductivity electrode was connected to the outlet of the central stream to obtain conductivity measurements.

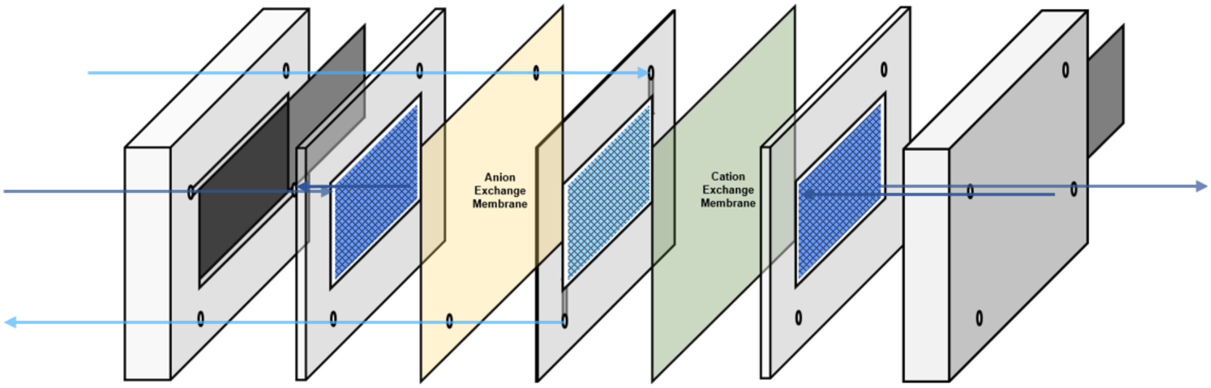

Figure S2. Sectional view of flow-cell setup for the multi-channel membrane capacitive deionization (MC-MCDI) experiments. The light blue arrows represent the flow path for the desalinating stream and the dark blue arrows represent the flow path for the higher salinity (100 mM NaCl) outer stream.

The deionization experiments were conducted in a similar fashion to that of MCDI with the addition of flowing 100 mM NaCl through the outer channels (represented by the dark blue arrows in **Figure S2**). The flowrate of the solution flowing through the outer channel was the same as the flowrate of the central stream.

R-MCDI: Endplates were assembled in a similar fashion to that of the MC-MCDI with both electrodes-spacer assemblies being overlayed by cation-exchange membranes to from the outer channel. Two 150 μm polycarbonate gaskets separated by an anion exchange membrane were sandwiched between the endplate assemblies to form the central desalinating streams as shown in **Figure S3**. Flow-through conductivity electrodes were connected at the outlets of both desalinating streams to obtain conductivity measurements.

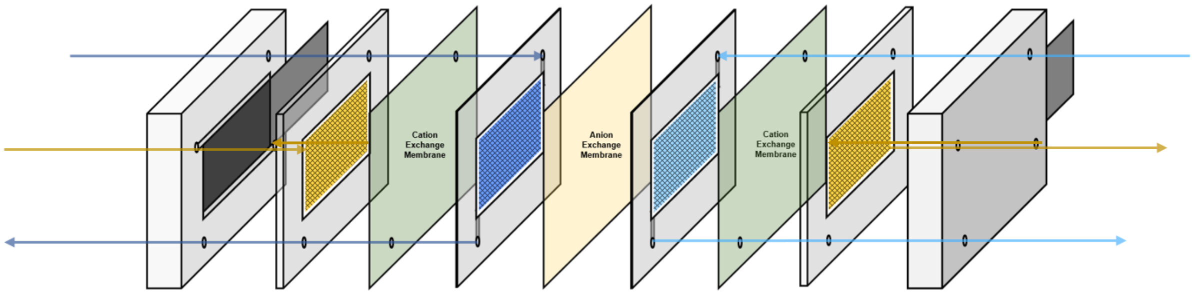

Figure S3. Sectional view of flow-cell setup for the redox capacitive deionization (R-MCDI) experiments. The light and dark blue arrows represent the flow path for the desalinating and concentrating streams, respectively. the yellow arrows represent the flow path for the redox-active electrolyte (50 mM Na_2SO_4 + 40 mM $K_3[Fe(CN)_6]$ + 40 mM $Na_4[Fe(CN)_6]$).

The outer channels were used to flow a solution mixture of 50 mM Na_2SO_4, 40 mM $K_3[Fe(CN)_6]$, and 40 mM $Na_4[Fe(CN)_6]$ (represented by the yellow arrows in **Figure S3**) which acted as the redox couple. A high flowrate of 10-20 mL·min^{-1} was used in the outer channel to maximize mass-transfer of redox-active species to the electrode surface. An influent 20 mM NaCl was allowed to flow through both the central desalinating streams (represented by the light and dark blue arrows in **Figure S3**). A constant current was applied to the flow-cell for 30 minutes, and the effluent conductivity measurements were logged.

The parameters used for conducting the deionization experiments on all the tested cell configurations are shown in **Table S1**.

Table S1. Parameters used while performing constant current deionization experiments on each architecture. The area of the electrode exposed to the electrolyte was 21 cm^2.

Applied Current (mA)	Voltage Window (V)	Flow Rate ($mL\cdot min^{-1}$)
10	0.0 - 0.8	1.0, 1.5, and 2.0
15	0.0 - 1.0	1.5, 2.0, and 2.5
20	0.0 - 1.2	2.0, 2.5, and 3.0

Longevity experiments: The longevity tests performed on the three different architectures utilized the exact same experimental setup as their respective deionization experiments. For the MCDI and MC-MCDI systems, 20 mM NaCl was allowed to flow through the central desalinating stream at a flowrate of 3 $mL\cdot min^{-1}$. The outer channel of the MC-MCDI was filled with 100 mM NaCl flowing at 3 $mL\cdot min^{-1}$. To simulate long-term usage, both systems were galvanostatically charged and discharged at 15 mA between 0.0 V and 1.0 V for 250 cycles. Electrochemical impedance spectroscopy (EIS) measurements were taken between every 50 cycles to observe how the resistance of the CDI architecture evolved over multiple cycles (see **Section S4**).

For the R-MCDI architecture, the redox-active compounds were recirculated in the outer channels at 15 $mL\cdot min^{-1}$ and 20 mM NaCl was passed through the two desalinating streams at 3 $mL\cdot min^{-1}$. Long-term usage was simulated by passing 15 mA current for ~50 hours. EIS measurements were taken at 10-hour intervals to observe the change in resistance of the system (see **Section S4**).

Section S2. Energy demand and salt adsorption capacity analysis.

Representative cell voltage and effluent concentration profile as a function of time for the MCDI architecture operated at a constant current of 20 mA and flowrate of 3 mL·min^{-1} are shown in **Figure S5** as an example for energy and salt adsorption capacity calculations.

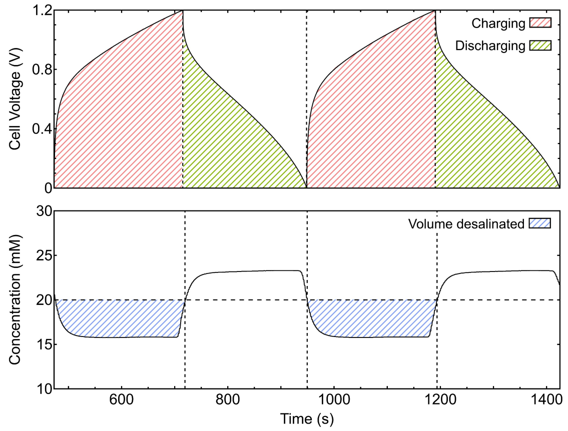

Figure S4. Representative voltage and effluent concentration profile for capacitive electrode-based deionization system.

The net volumetric energy (E_v) consumed over the two deionization cycles is given by the following integral:

$$E_v = \frac{1}{V_D}\left[\int I \cdot V(t) \cdot dt\ (Red) + \int -I \cdot V(t) \cdot dt\ (Green)\right] \qquad \text{(S1)}$$

where V_D is the volume of deionized water, I is the applied constant current, and $V(t)$ is the cell-voltage as a function of time. The volume of deionized effluent produced is calculated as follows:

$$V_D = \int Q(t) \cdot dt\ (Blue) \qquad \text{(S2)}$$

where $Q(t)$ is the flowrate used when performing the deionization experiment. The salt adsorption capacity (SAC, $mg_{NaCl}/g_{electrode}$) of the system was calculated as follows:

$$SAC = \frac{\left[\int Q(t) \cdot V(t) \cdot dt\ (Blue)\right] \cdot M_{NaCl} \cdot 1000}{2 \cdot n \cdot M_{electrode}} \qquad \text{(S3)}$$

where M_{Nacl} is the molar mass of NaCl (58.55 $g_{NaCl}\cdot mol^{-1}$), $M_{electrode}$ is the mass of the electrode in grams, n is the number of cycles, the two in the denominator is to account for having two electrodes, and the 1000 is a conversion factor for grams to milligrams.

Section S3. Procedure for calculating volumetric energy demand and productivity for 5 mM reduction in influent concentration.

To calculate the energy demand and productivity for a concentration reduction of 5 mM, we first determined the energy demand and productivity for each experiment conducted (nine for each architecture). We then plotted the E_v and P as a function of concentration reduction (ΔC, mM) as shown in **Figure S5**.

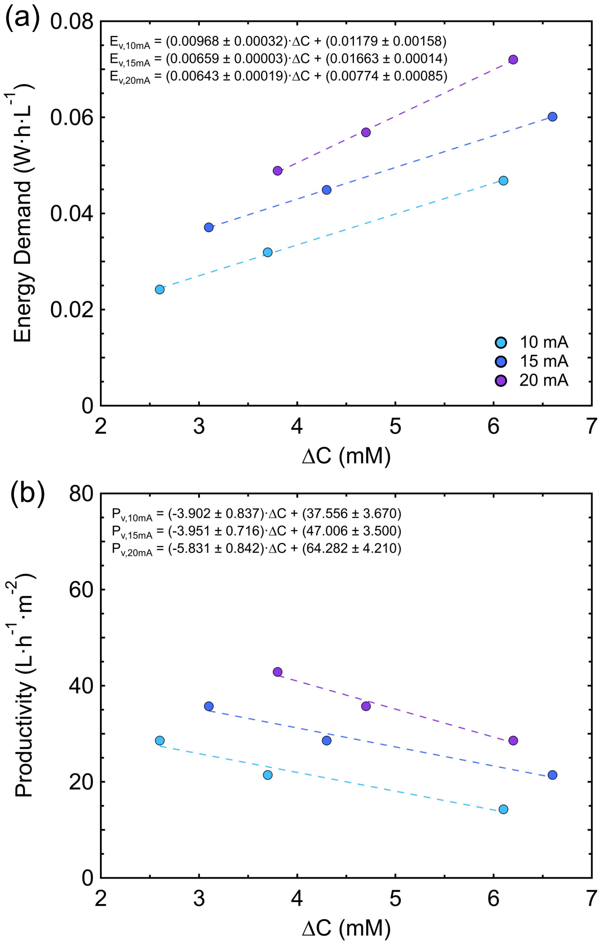

Figure S5. Plots of **(a)** volumetric energy demand and **(b)** productivity as a function of effluent concentration reduction.

Linear regression equations are determined for energy demand vs. ΔC and productivity vs. ΔC at each current density (i.e., 10, 15 and 20 mA). The regression equations are then used to calculate the energy demand and productivity for ΔC of 5 mM. The energy demand and productivity are then plotted to make **Figure 2**a.

Section S4. Electrochemical impedance (EIS) spectroscopy experiments.

EIS measurements were taken over the course of the longevity experiments for each cell architecture. The solutions were allowed to flow as is when the EIS test was being conducted. The EIS test comprised of applying a sine wave potential of 10 mV amplitude between a frequency range of 700 kHz to 20 mHz. For both the M-CDI and MC-MCDI architectures, EIS tests were conducted in 50 cycle intervals (i.e., the EIS measurements were taken after 50th, 100th, 150th, 200th and 250th cycle). The flow-cell was allowed to rest at OCV for 10 minutes before each of the EIS measurements were taken. The Nyquist plots for the MCDI and MC-MCDI cell configurations are shown in **Figure S6** (panels a and b).

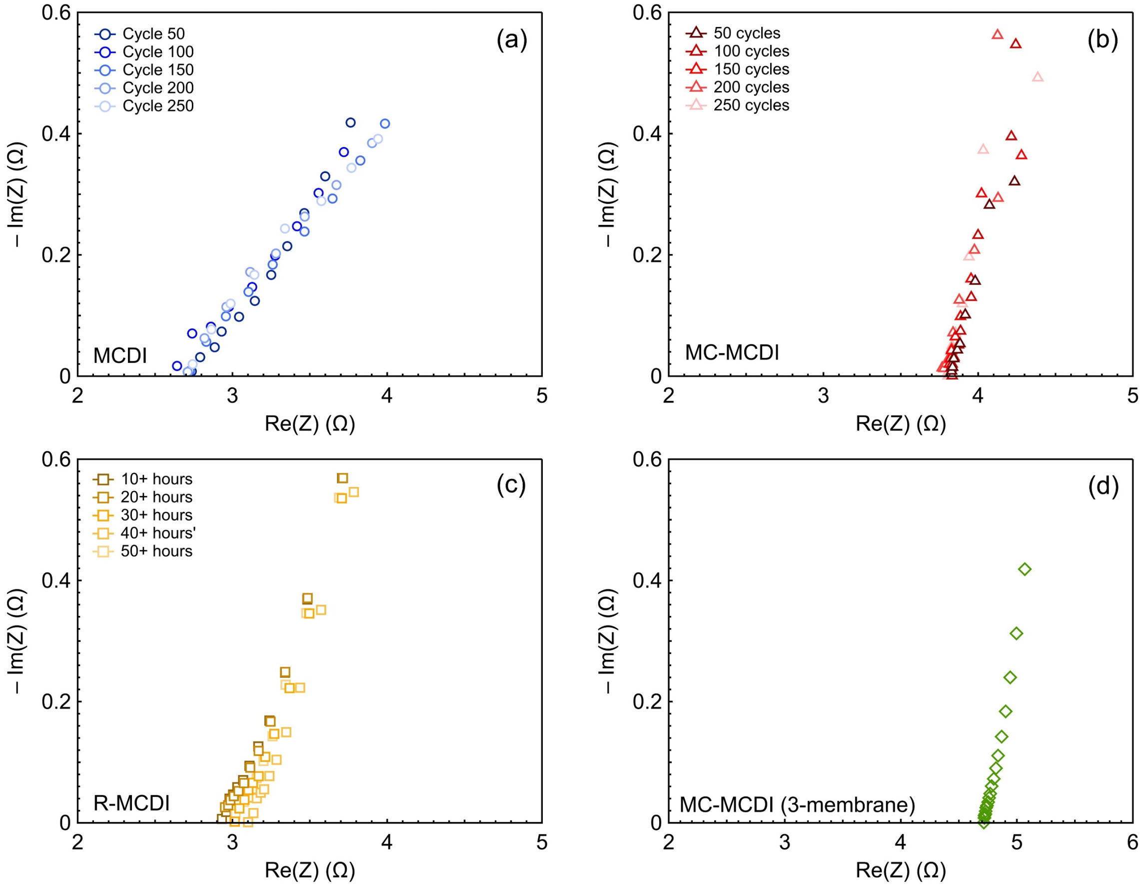

Figure S6. Nyquist plots of electrochemical impedance spectroscopy experiments conducted on **(a)** MCDI, **(b)** MC-MCDI, and **(c)** R-MCDI. The impedance spectra were collected at 50 cycle intervals for the MCDI and MC-MCDI systems while performing the longevity tests. For the R-MCDI system, the impedance spectra were collected at 10-hour intervals when performing the longevity test. **(d)** Nyquist plot for MC-MCDI system with three membranes.

For the R-MCDI architecture, the EIS tests were conducted 10-hour intervals (i.e., the EIS measurements were taken after the 10th, 20th, 30th, 40th, and 50th hour of constant current application). Similar to the previous two architectures, the flow-cell was allowed to rest at the open circuit voltage for 10 minutes before the EIS measurements were taken (**Figure S6c**).

Longevity tests were not performed on the three-membraned MC-MCDI cell and the EIS experiment was conducted with 100 mM NaCl flowing through the outer channels and 20 mM NaCl flowing through the central channels at 15 $mL·min^{-1}$ and 3 $mL·min^{-1}$, respectively. The three-membraned MC-MCDI cell was charged and discharged for 10 cycles and was allowed to rest at OCV for 10 minutes before performing the EIS test. The resulting Nyquist plot is shown in **Figure S6d**.

Section S5. Binder dissolution and its effect on longevity test for the MC-MCDI system.

Longevity tests on the MC-MCDI system were initially performed with the binder between the electrode and the current collector. However, after 250 charge and discharge cycles, we observed that the high salinity electrolyte (100 mM NaCl) contacting the electrode had turned cloudy. We also observed an anomalous trend of increasing capacity in the initial few cycles which was followed by gradual stabilization and then gentle decrease of the capacity as seen in **Figure S7**.

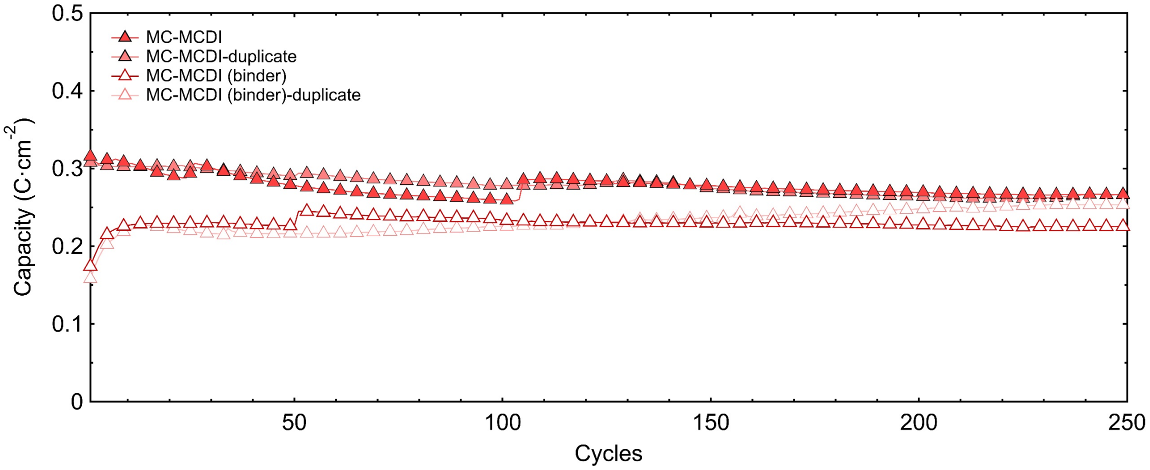

Figure S7. Capacity retention of MC-MCDI system, the closed triangular markers represent the MC-MCDI system with no binder and the open triangular markers represent the MC-MCDI system with binder.

Analyzing the solution with UV-vis spectroscopy (Shimadzu UV-1800 spectrophotometer) yielded an absorption peak at 206 nm, consistent with the binder between the electrode and current collector dissolving.(1) We suspect that the dissolution of binder increased the amount of electrode surface exposed to the electrolyte, resulting in the increasing capacity seen in **Figure S7**. To determine if the binder dissolution caused this increase, we performed the longevity test on an MC-MCDI setup without any binder between the electrode and collector. The MC-MCDI system with no binder (**Figure S7**) did not show an initial increase in capacity and exhibited a very gradual decrease in its capacity over 250 cycles. When comparing the long-term capacity retention of both the MC-MCDI (with and without binder) systems, we noticed that the capacity seemed to converge towards 0.25 C·cm^{-2}.

Reference

1. Elashmawi IS, Hakeem NA. Effect of PMMA addition on characterization and morphology of PVDF. Polymer Engineering & Science. 2008;48(5):895-901.